Cancer Research

Mdm2 and Aurora Kinase A Inhibitors Synergize to Block Melanoma Growth by Driving Apoptosis and Immune Clearance of Tumor Cells

Anna E. Vilgelm[1,2], Jeff S. Pawlikowski[1,2], Yan Liu[1,2], Oriana E. Hawkins[1,2], Tyler A. Davis[3], Jessica Smith[4], Kevin P. Weller[5], Linda W. Horton[1,2], Colt M. McClain[6], Gregory D. Ayers[7], David C. Turner[8], David C. Essaka[8], Clinton F. Stewart[8], Jeffrey A. Sosman[9], Mark C. Kelley[10], Jeffrey A. Ecsedy[11], Jeffrey N. Johnston[3], and Ann Richmond[1,2]

Abstract

Therapeutics that induce cancer cell senescence can block cell proliferation and promote immune rejection. However, the risk of tumor relapse due to senescence escape may remain high due to the long lifespan of senescent cells that are not cleared. Here, we show how combining a senescence-inducing inhibitor of the mitotic kinase Aurora A (AURKA) with an MDM2 antagonist activates p53 in senescent tumors harboring wild-type 53. In the model studied, this effect is accompanied by proliferation arrest, mitochondrial depolarization, apoptosis, and immune clearance of cancer cells by antitumor leukocytes in a manner reliant upon Ccl5, Ccl1, and Cxcl9. The AURKA/MDM2 combination therapy shows adequate bioavailability and low toxicity to the host. Moreover, the prominent response of patient-derived melanoma tumors to coadministered MDM2 and AURKA inhibitors offers a sound rationale for clinical evaluation. Taken together, our work provides a preclinical proof of concept for a combination treatment that leverages both senescence and immune surveillance to therapeutic ends. *Cancer Res; 75(1); 181–93. ©2014 AACR.*

Introduction

Metastatic melanoma is a highly aggressive disease and one of the most challenging malignancies to treat. MAPK pathway targeting with inhibitors of BRAF (vemurafenib and dabrafenib) and/or MEK (trametinib) provide a therapeutic option for nonresectable melanoma tumors driven by oncogenic BRAF kinase ($BRAF^{V600E}$; ref. 1). However, the majority of patients eventually relapse (median progression-free survival is 6 months for dabrafenib alone and 9.4 months for dabrafeneb and trametinib combination, with a median overall survival of 23.8 months; refs. 1–5). Furthermore, about half of melanoma tumors are $BRAF^{WT}$ and thus are not eligible for BRAF targeted therapies. New therapeutic options are needed for patients with $BRAF^{WT}$ and BRAF inhibitor-resistant tumors.

Aurora kinase A (AURKA), an essential mitotic kinase indispensable for cell proliferation, is a promising therapeutic target in cancer. The AURKA inhibitor MLN8237 (alisertib) is now being evaluated in several clinical trials for melanoma and other malignancies, though as a single agent the benefit has been somewhat limited (clinicaltrials.gov; ref. 6). In our preclinical study, MLN8237 treatment markedly slowed the growth of >75% of patient-derived metastatic melanoma tumors independent of *BRAF* and *NRAS* mutational status. AURKA inhibition induced tumor senescence, but not apoptosis (7). To improve treatment efficacy, we sought to identify a potential therapeutic partner for the AURKA inhibitor that is capable of activating death pathways in senescent melanoma cells.

The inactivation of the proapoptotic cell fate regulator p53 is considered indispensable for oncogenic transformation (8). In mouse melanoma models either genetic loss or downregulation of p53 through p14/Arf inactivation or MDM4 overexpression cooperated with oncogenic kinases $Braf^{V600E}$ and Nras in melanoma tumorigenesis (9–11). Overexpression of p53 due to Mdm4 inactivation, in turn, blocked HRAS-driven melanoma progression (12). Thus, restoring p53 function is a viable strategy for melanoma intervention especially because mutations and allelic loss of *TP53* are relatively rare in those malignancies (16%–19%; refs. 13, 14).

The *CDKN2A* locus (*INK4a*/*ARF*) is often compromised by deletions, promoter methylation, or genetic mutations in both sporadic and hereditary melanoma (13, 15, 16). One of its products, p14/ARF, is a negative regulator of MDM2 ubiquitin ligase that controls p53 degradation (17). Loss of p14/ARF upon

[1]Tennessee Valley Healthcare System, Department of Veterans Affairs, Vanderbilt University Medical Center, Nashville, Tennessee. [2]Department of Cancer Biology, Vanderbilt University Medical Center, Nashville, Tennessee. [3]Department of Chemistry and Vanderbilt Institute of Chemical Biology, Vanderbilt University Medical Center, Nashville, Tennessee. [4]Meharry Medical College, Nashville, Tennessee. [5]Flow Cytometry Shared Resource, Vanderbilt University Medical Center, Nashville, Tennessee. [6]Department of Pathology, Microbiology, and Immunology, Vanderbilt University Medical Center, Nashville, Tennessee. [7]Division of Cancer Biostatistics, Vanderbilt University Medical Center, Nashville, Tennessee. [8]Department of Pharmaceutical Sciences, St. Jude Children's Research Hospital, Memphis, Tennessee. [9]Division of Hematology/Oncology, Department of Medicine, Vanderbilt University Medical Center, Nashville, Tennessee. [10]Division of Surgical Oncology, Department of Surgery, Vanderbilt University Medical Center, Nashville, Tennessee. [11]Takeda Pharmaceuticals International Co., Cambridge, Massachusetts.

Note: Supplementary data for this article are available at Cancer Research Online (http://cancerres.aacrjournals.org/).

Corresponding Author: Ann Richmond, Vanderbilt University School of Medicine, PRB 771, 2220 Pierce Avenue, Nashville, TN 37232. Phone: 615-343-7777; Fax: 615-936-2911; E-mail: ann.richmond@vanderbilt.edu

doi: 10.1158/0008-5472.CAN-14-2405

CDKN2A inactivation has been implicated in disabling p53 tumor-suppressor activity in melanoma, as illustrated by the mutually exclusive pattern of *CDKN2A* and *TP53* mutations (13, 18). Therefore, targeting MDM2, which is downstream of p14/ARF, could restore compromised p53 activity in melanoma.

Apart from *CDKN2A* inactivation, overexpression of MDM4 has also been shown to contribute to p53 inactivation in a substantial proportion of human melanomas (11). It is plausible that cotargeting MDM4 with MDM2 may achieve robust p53 induction in these tumors. However, currently there are no specific inhibitors of MDM4 or dual MDM2/MDM4 inhibitors available for clinical testing. In contrast, compounds that specifically target p53 interaction with MDM2 show promising results in clinical trials (19). However, a recent study indicated that MDM2 antagonism alone may not be sufficient to restore p53-mediated tumor suppression in melanoma. The therapeutic efficacy of MDM2 inhibition was enhanced by cotargeting BRAF and iASPP, but complete abrogation of tumor growth was not achieved (20).

Induction of senescence has been found to be essential for the regression of established tumors upon genetic p53 reconstitution, as it promotes immune-mediated tumor clearance (21). Hence, we tested whether combining p53-activating MDM2 antagonist with a senescence-inducing AURKA inhibitor can benefit melanoma therapy.

Materials and Methods

Chemical reagents and cell culture

For *in vitro* studies, stock solutions of (−)-Nutlin-3 (30 mmol/L) and MLN8237 (20 mmol/L) were prepared in DMSO. The pan-caspase inhibitor Z-VAD-FMK was obtained from Molecular Probes (Eugene). Cisplatin was purchased from Sigma-Aldrich and a 10 mmol/L stock solution was prepared in DMSO. SK-Mel5, HS294T, SK-Mel28 human melanoma cells, and B16F0 mouse melanoma cells were obtained from the ATCC. Cells were cultured in DMEM/F12 media supplemented with 10% FBS, 100 U/mL penicillin and 100 μg/mL streptomycin.

Animal studies

Experiments were conducted in accordance with Vanderbilt University Animal Care and Use Committee guidelines (protocol M/10/034). To establish tumors, 2×10^6 SK-Mel5 or 4×10^4 B16F0 cells were injected s.c. in both flanks of BALB/c nu/Foxn1 athymic nude mice or C57Bl/6 mice (Harlan–Sprague–Dawley), respectively. Generation of patient-derived xenograft (PDX) was approved by the Institutional Review Board and has been described previously (22). Mutational status of *TP53* was determined by direct exon sequencing with primers available from IARC TP53 Database (R16, November 2012). (−)-Nutlin-3 was synthesized as described previously (23). MLN8237 was provided by Takeda Pharmaceuticals. At least 5 mice per treatment group were used. Drugs were given by oral gavage in 2% Klucel, 0.5% Tween 80 [(−)-Nutlin-3], and water (MLN8237). MLN8237 was administered once a day; (−)-Nutlin-3 was given twice daily in experiments with B16F0 melanoma tumors, PDXs of patients 2 and 3, and once a day on other experiments. Because of the aggressiveness of B16F0 tumors, treatment began when they were palpable. In all other experiments treatment began when tumors were 100 mm^3. Animal weight and tumor dimensions were measured two to four times weekly. Tumor volumes were calculated as 0.5 × length × width × width. In all animal experiments, the endpoint was when tumors in any of the treatment groups exceeded 15 mm in diameter, at which time mice in all treatment groups were sacrificed and tumors collected for downstream analyses, for example, Western blot analysis, flow cytometry, qPCR, immunofluorescence, immunohistochemistry (IHC), hematoxylin and eosin (H&E), and SA-β-Gal staining.

(−)-Nutlin-3 and MLN8237 pharmacokinetics

Blood and tumor samples were harvested over a time course of 24 hours after drug administration ($n = 4$/time point). (−)-Nutlin-3 concentrations were assayed by validated high-performance liquid chromatography electrospray ionization tandem mass spectrometry (LC/ESI/MS-MS) assay (24). Detailed explanation of MLN8237 analysis and sample preparation is given in Supplementary Experimental Procedures. (−)-Nutlin-3 and MLN8237 concentration–time data were fitted by a two-compartment plasma model coupled to a perfusion-limited tumor compartment (Supplementary Fig. S1), using a nonlinear mixed effects pharmacokinetic modeling approach implemented in NONMEM (25). Estimated pharmacokinetic parameters are shown in Supplementary Table S1. The proportional residual error term was fixed to 10%, tumor volume was fixed to 0.339 cm^3 (1.65×10^{-5} mL/kg), and tumor blood flow (Q_t) was fixed to 5.8% of cardiac input (approximate blood flow to the skin; ref. 26). The $AUC_{0-24\ h}$ was estimated on the basis of the individual simulated concentration–time curves using the trapezoidal method.

Western blotting, viability, apoptosis, flow cytometry, immunofluorescence and SA-β-Gal analyses, and antibodies are described in detail in Supplementary Experimental Procedures.

Statistical analyses

Unless otherwise stated, ANOVA followed by the Dunnett test for pair-wise comparisons was used. To compare mouse treatment groups, the natural log of average tumor burden over time was analyzed using mixed models ANOVA for repeated measures with an AR(1) covariance structure for random effects. The log transformation was used to correct for heteroscedacity inherent in tumor growth models. The AR(1) covariance structure was uniformly selected across all xenograft models, based on the Akaike information criteria measure. Quadratic and interaction effects were included as appropriate based on the likelihood ratio test. Group means and their differences were estimated and compared using linear contrasts. Group differences in tumor volume were considered statistically significant for P values smaller than their Bonferroni correction that protects the per-experiment type I error rate <5%. The results of the statistical comparisons are specified on figures as *, $P < 0.05$; **, $P < 0.01$; ***, $P < 0.001$; and ns, $P > 0.05$.

Results

MDM2 antagonism limits lifespan of senescent melanoma cells

Senescent cells can acquire resistance to certain proapoptotic stimuli, including serum withdrawal, radiation, oxidative stress, and treatment with DNA-damaging drugs (27–30). Notably, the senescence-associated resistance to apoptosis has been linked to impaired activation of p53 (29, 31). Therefore, we hypothesized that activation of p53 in senescent cells may restore death pathway functionality. To initiate senescence, the AURKA inhibitor MLN8237 was used (7, 32). (−)-Nutlin-3 (Nutlin-3a) was used

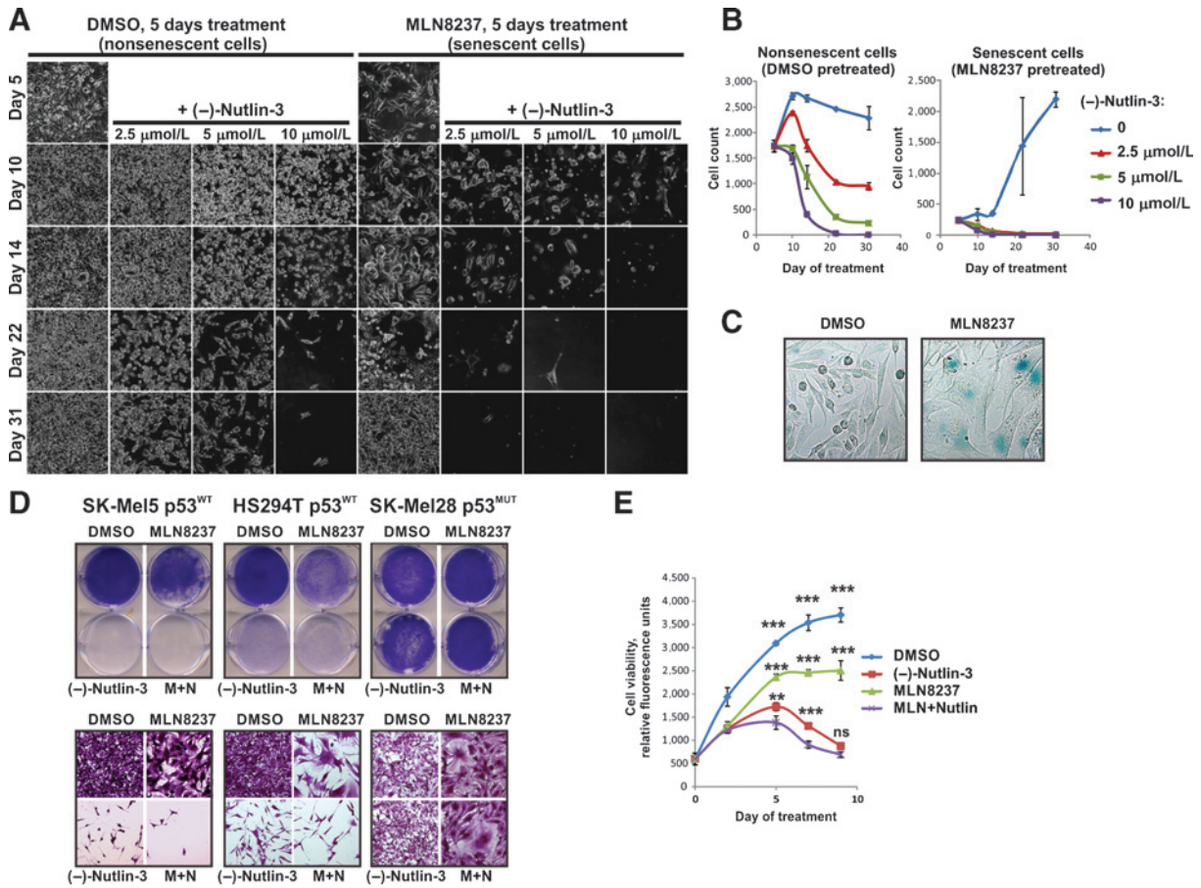

Figure 1.
Inhibition of MDM2 limits survival of senescent melanoma cells. A, microphotographs of live SK-Mel5 melanoma cells pretreated with 1 μmol/L of MLN8237 or DMSO followed by treatment with (−)-Nutlin-3 as indicated. B, quantification of experiments shown in A. Average number of cells per microphotograph ± SD is shown. C, SA-β-Gal staining of SK-Mel5 cells treated with 1 μmol/L MLN8237 or DMSO for 5 days. D, crystal violet staining shows cell density on macro- (top) and microscopic (bottom) levels. Cells were treated with (−)-Nutlin-3 (10 μmol/L), MLN8237 (1 μmol/L), combination of both (M+N), or vehicle for 7 days. E, time-dependent changes in viability of SK-Mel5 cells treated as in A using the MultitoxFluor Kit. Experiments were performed twice in triplicate; average viability ± SEM of a representative experiment is shown. Two-way ANOVA with the Bonferroni posttest was used for data analysis. Statistical analysis: **, $P < 0.01$; ***, $P < 0.001$; ns, not significant, $P > 0.05$.

to induce expression of endogenous p53 by inhibiting MDM2–p53 interaction (33). We observed dose-dependent cytotoxicity of (−)-Nutlin-3 in both senescent (MLN8237 pretreated) and nonsenescent (vehicle pretreated) cells (Fig. 1A and B). MLN8237-pretreated cells remained static but viable after drug withdrawal. Notably, without p53 activation, some cells were able to escape senescence and regain their proliferative potential, which resulted in culture outgrowth by day 31. In contrast, all (−)-Nutlin-3–treated senescent cells died before any of them could regrow. The induction of senescence was confirmed using SA-β-Gal (senescence-associated β-galactosidase) staining (Fig. 1C). This suggests that p53 activation prevents senescence escape by reducing the lifespan of senescent cells. We also tested concurrent AURKA and MDM2 inhibition. Melanoma cells remained viable after a week of continuous exposure to MLN8237, suggesting a mostly cytostatic response (Fig. 1D and E). In contrast, p53 activation by (−)-Nutlin-3 administered alone or in combination with MLN8237, killed $p53^{WT}$ melanoma cells (Fig. 1E). These results show that the reduction in viable tumor cells with combined treatment is a result of both proliferative arrest caused by AURKA inhibition and cell death driven by MDM2 antagonism. Importantly, (−)-Nutlin-3 did not affect viability of cells expressing nonfunctional mutated p53 (Fig. 1D) or cells with p53 knockout (Supplementary Fig. S2A), demonstrating the lack of p53-independent/off-target effects under these experimental conditions.

p53 activation induces caspase-independent cell death in senescent melanoma cells

Because we have previously characterized the mechanisms by which AURKA inhibition induced melanoma senescence (7), we focused here on consequences of AURKA inhibition combined with MDM2 antagonism. As expected, (−)-Nutlin-3–induced accumulation of p53 and its transcriptional targets p21, PUMA, BAX, and MDM2 in $p53^{WT}$ cells (SK-Mel5 and Hs294T; Fig. 2A, Supplementary Fig. S2B). Of note, MDM2 accumulation does not cause p53 degradation in the context of (−)-Nutlin-3 treatment because this drug interferes with the binding of MDM2 to p53. Consistent with high specificity of this drug, the level and activity of p53 was unaffected by (−)-Nutlin-3 in $p53^{MUT}$ SK-Mel28 cells (Fig. 2A). Interestingly, treatment with the AURKA inhibitor induced p53

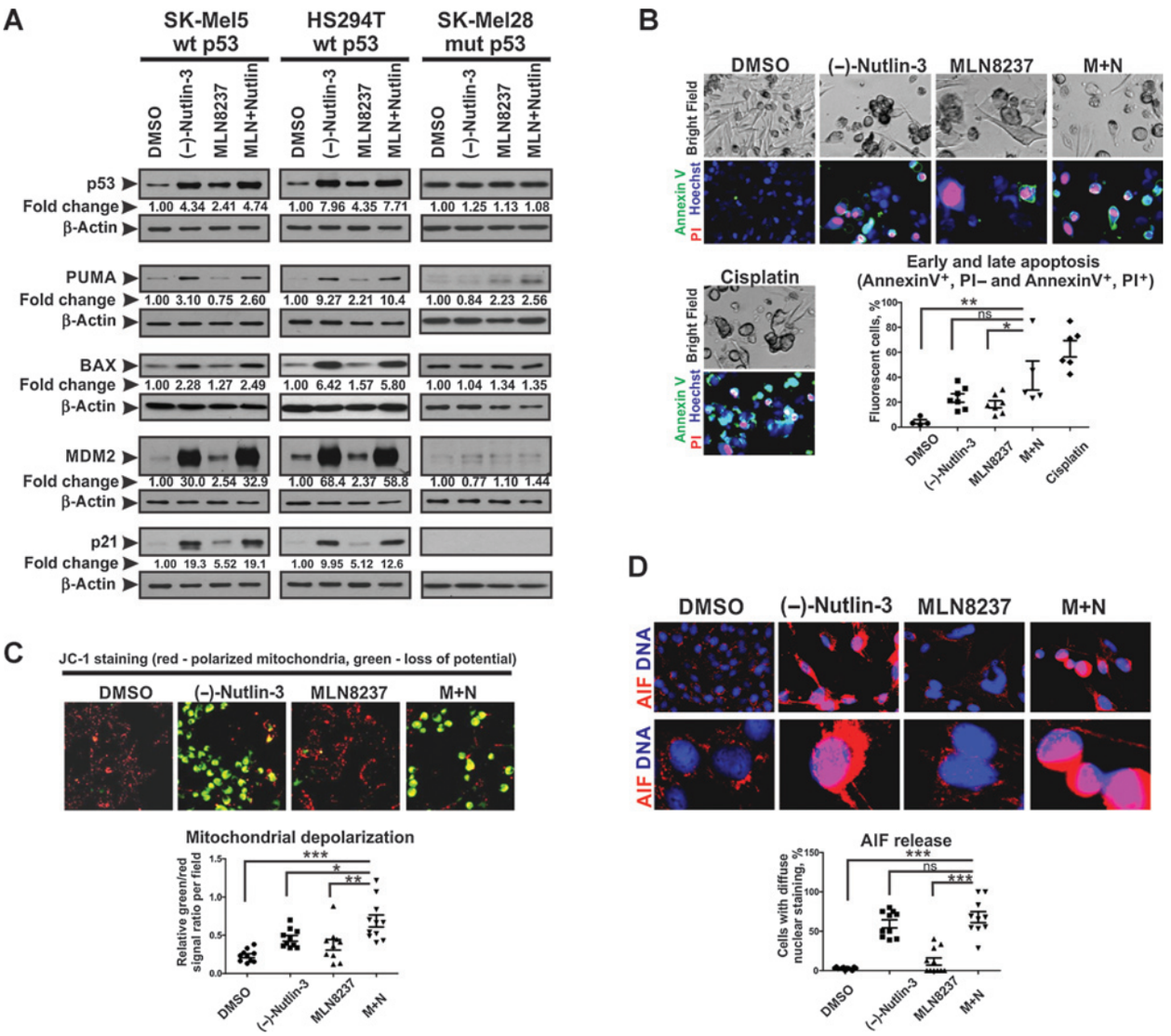

Figure 2.

MDM2 antagonism induces mitochondrial-mediated apoptosis in senescent melanoma cells. A, Western blot analysis of p53 levels and expression of p53 target genes after 5 days of treatment with (−)-Nutlin-3 (10 μmol/L), MLN8237 (1 μmol/L), combination of both, or vehicle. Numbers are average β-actin–normalized densitometry values from three independent experiments. B, analysis of apoptosis using Annexin V–FITC and propidium iodide (PI) staining . SK-Mel5 cells were treated for 5 days as in A. Bottom, the percentages of apoptotic cells per random microscope field. C, mitochondrial membrane potential in cells treated as described in A was analyzed using JC-1 dual emission dye. Fluorescence of cells in red (polarized mitochondria) and green (loss of mitochondrial membrane potential) channels were evaluated. Graph, relative green to red signal ratios in random fields. D, immunofluorescence staining of AIF in SK-Mel5 cells treated as described in A. Bottom, the percentages of cells with nuclear AIF staining in random fields. The Kruskal–Wallis test with Dunn multiple comparison was applied. Experiments were performed at least three times with consistent results. Images were quantified with ImageJ software. Statistical analysis: *, $P < 0.05$; **, $P < 0.01$; ***, $P < 0.001$; ns, not significant, $P > 0.05$.

accumulation in $p53^{WT}$-expressing melanoma cells, although it was less effective compared with (−)-Nutlin-3 (Fig. 2A).

p53 stabilization by (−)-Nutlin-3–induced apoptosis in $p53^{WT}$ melanoma cells (Fig. 2B). p53 activates expression of key proapoptotic mitochondrial proteins, including PUMA, NOXA, and BAX, that promote mitochondrial membrane depolarization, leading to release of apoptotic effectors (34). Indeed, we found that p53 activation by (−)-Nutlin-3 alone and in combination with MLN8237 increased expression of PUMA and BAX (Fig. 2A), which was accompanied by the decrease in mitochondrial membrane potential (Fig. 2C). Interestingly, despite the strong evidence of apoptosis, cleavage of caspase-3 was not detected in cells treated with (−)-Nutlin-3 (Supplementary Fig. S2C). In addition, treatment with pan-caspase inhibitor did not interfere with cytotoxic response to p53 activation (Supplementary Fig. S2D). These data argue for a caspase-independent mechanism of (−)-Nutlin-3–induced apoptosis. Consistently, we found that treatment of melanoma cells with (−)-Nutlin-3–induced activation, mitochondrial release, and nuclear translocation of apoptosis-inducing factor (AIF; Fig. 2D), which is a known effector of caspase-

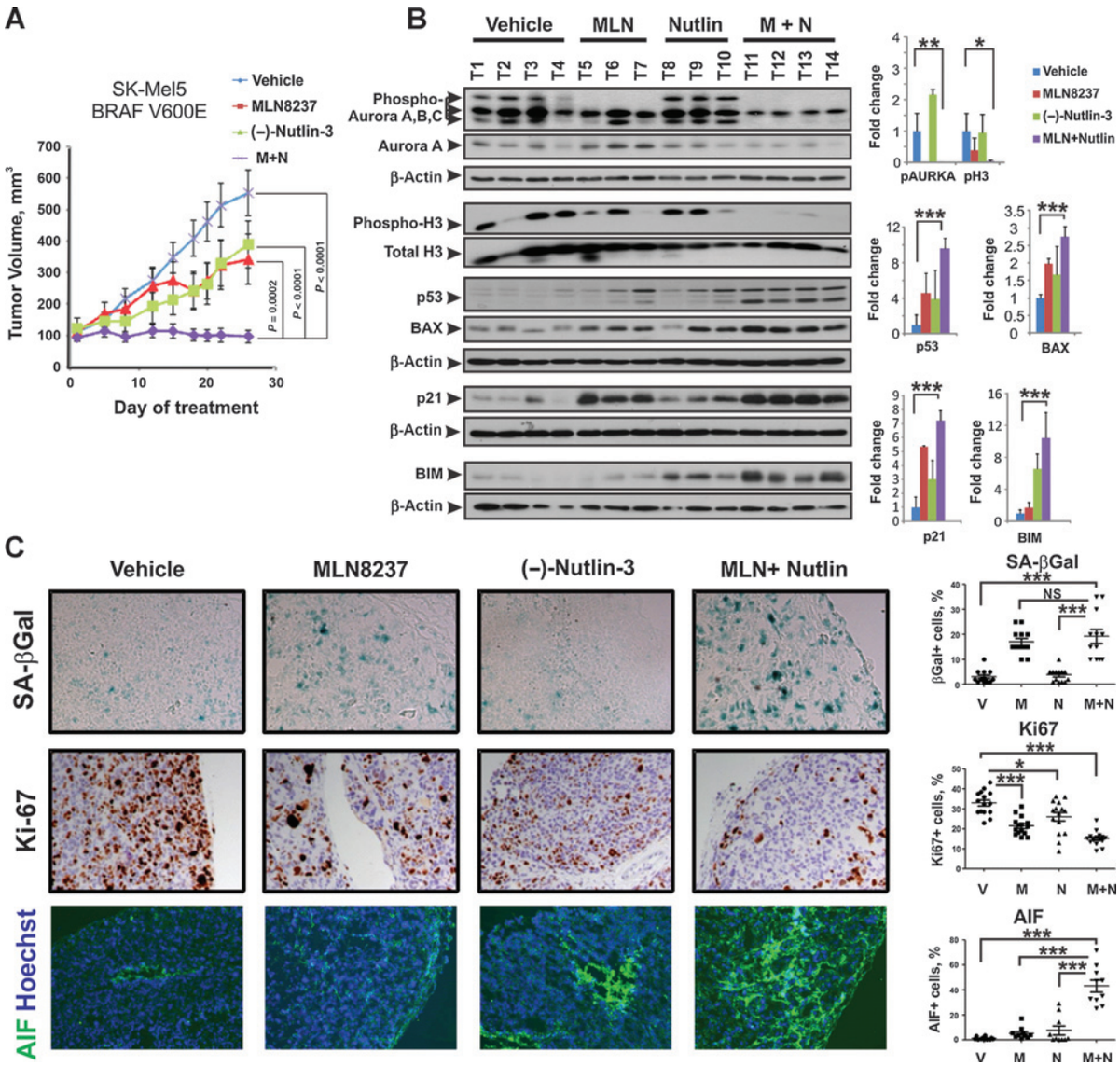

Figure 3.
Cotargeting AURKA and MDM2 blocks melanoma growth *in vivo*. A, mice bearing SK-Mel5 xenografts received daily treatments with (−)-Nutlin-3 (200 mg/kg), MLN8237 (30 mg/kg), combination of both, or vehicle control. Tumor volume changes over time are shown. B, Western blot analysis of tumors (T) described in A. Expression was normalized to β-actin based on densitometry analysis and the average fold changes ± SD in different treatment groups over the placebo group were plotted (right). C, representative results of SA-βGal, Ki-67, and AIF staining in tumors described in A. Percentages of AIF and Ki-67–positive cells were quantified using ImageJ software; SA-β-Gal staining was scored by pathologist in a blind fashion. Five random fields of two to three tumors were evaluated in each treatment group. V, vehicle; N, (−)-Nutlin-3; M, MLN8237; M+N, combined MLN8237, and (−)-Nutlin-3 treatment. Statistical analysis: *, $P < 0.05$; **, $P < 0.01$; ***, $P < 0.001$; ns, not significant, $P > 0.05$.

independent apoptosis (35). Collectively, these results demonstrate that prolonged activation of p53 in melanoma cells initiates caspase-independent programmed cell death driven by mitochondrial depolarization and AIF activation.

MDM2 and AURKA antagonists work in concert to activate p53 and block melanoma tumor growth *in vivo*

Xenograft of human melanoma cells was used to evaluate responses to (−)-Nutlin-3 and/or MLN8237 *in vivo*. Although single-agent treatments only partially inhibited tumor progression, combined (−)-Nutlin-3 and MLN8237 treatment fully blocked tumor growth (Fig. 3A). As expected, MLN8237 inhibited AURKA activity, shown by loss of AURKA autophosphorylation in tumor lysates (Fig. 3B). This resulted in inhibition of cancer cell proliferation and induction of senescence, based upon the decrease of proliferative markers phosphorylated histone H3 and Ki-67 and the increase in SA-β-Gal activity (Fig. 3B and C). Consistent with our *in vitro* findings (Fig. 2A), MLN8237 treatment caused moderate induction of p53 (Fig. 3B). The lower of the two bands detected by the human p53-specific antibody may represent an alternative p53 isoform (36). Interestingly, although in cultured cells p53 levels were greatly elevated by MDM2

inhibitor, *in vivo* p53 activation by (−)-Nutlin-3 was modest, resulting in limited induction of p53 target genes p21, BAX, and apoptosis, based on AIF staining (Fig. 3B and C). To gain better understanding of these findings, we evaluated tumor cell expression of p53. Only 11% of cells in the (−)-Nutlin-3–treated tumors had elevated p53 (compared with 3%–6% in untreated control tumors; Supplementary Fig. S3). This is much lower than the results obtained *in vitro* where 100% of cells showed strong p53 induction (Supplementary Fig. S2B). This suggests that systemic administration of (−)-Nutlin-3 may not target all tumor cells equally, as opposed to *in vitro* cell culture conditions. In this case, cells unaffected by (−)-Nutlin-3–induced apoptosis would have proliferative advantage, and therefore addition of the cytostatic AURKA antagonist may promote (−)-Nutlin-3 efficacy. Indeed, we found that p53 activation and expression of p53 targets p21 and BAX was much more robust after combined MLN8237 and (−)-Nutlin-3 treatment in comparison with single-agent therapies (Fig. 3B). Up to 50% of tumor cells showed strong p53 staining in the combination treatment group (Supplementary Fig. S3). Similar to p53 levels, about 50% of tumor cells showed induction of the apoptosis marker AIF after combined MLN8237 and (−)-Nutlin-3 treatment, compared with no more than 15% after treatment with (−)-Nutlin-3 alone (Fig. 3C). Accumulation of the proapoptotic molecule BIM_{EL} in the tumor lysates of the MLN8237 and (−)-Nutlin-3–treated mice confirmed the induction of apoptosis (Fig. 3B). We also detected downregulation of proliferation markers phospho-H3 and Ki67 after combined MDM2 and AURKA inhibition consistent with higher p21 levels, indicating enhanced antiproliferative effect (Fig. 3B and C). These results show that MDM2 antagonism and AURKA inhibition cooperate to activate p53, induce cell death, and inhibit cell proliferation *in vivo*.

AURKA and MDM2 antagonism promotes tumor immune infiltration

Immune cells have been shown to target senescent tumor cells overexpressing p53 (21). To assess the effect of AURKA and MDM2 inhibitors on the antitumor immune response, we used an immunocompetent melanoma model in which B16F0 tumors are grown in syngeneic C57Bl/6 mice. *In vitro*, B16F0 cells showed decreased viability and induction of apoptosis in response to treatment with either drug, but the cytotoxic effect was most prominent with the combined treatment (Supplementary Fig. S4A and S4B). *In vivo*, MLN8237 alone partially inhibited tumor growth whereas (−)-Nutlin-3 showed no significant antitumor activity. Strikingly, combined (−)-Nutlin-3 and MLN8237 treatment elicited remarkable responses, completely blocking growth of aggressive B16 tumors (Fig. 4A and B). Drug responses in (−)-Nutlin-3 and MLN8237–treated tumors were associated with high p53 levels and increased expression of p53 transcriptional targets, such as proapoptotic molecules Bax and Puma and cell-cycle arrest mediator p21 (Fig. 4C and D).

Consistent with limited antitumor activity, p53 was not strongly induced upon treatment with (−)-Nutlin-3 (Fig. 4D). Although the resistance of B16 tumors to MDM2 inhibitor (−)-Nutlin-3 has been previously reported, the mechanism has not been determined (20). We found that microvessel density was decreased in tumors treated with (−)-Nutlin-3 alone (Supplementary Fig. S5). This is consistent with the study showing that (−)-Nutlin-3 limits vessel formation *in vivo* by inhibiting migration, proliferation, and survival of endothelial cells (37). Inadequate blood supply, in turn, has been shown to cause uneven distribution of anticancer drugs within tumor and cause drug resistance (38–40). Therefore, cells in poorly vascularized areas can be protected from exposure to drugs, resulting in a low overall level of p53 activation. The antiangiogenic effect of (−)-Nutlin-3 was not evident in combination with MLN8237 (Supplementary Fig. S5). This may be due to antiproliferative activity of MLN8237, which reduces the need for neoangiogenesis.

We have previously reported that targeting AURKA induces infiltration of immune cells into the tumor (7). Here, we found that combined MDM2 and AURKA inhibition further promoted tumor infiltration by host immune cells (Fig. 4E). Both lymphoid and myeloid cells accumulated in (−)-Nutlin-3 and MLN8237-treated tumors. The numbers of natural killer (NK) cells, macrophages, and antigen-presenting dendritic cells (DC) increased most prominently (Fig. 4F). These changes were present only at tumor sites and were not seen in either bone marrow or spleen (Supplementary Fig. S6A and S6B). In fact, the numbers of DCs and macrophages were decreased in the spleens of animals treated with the (−)-Nutlin-3 and MLN8237 combination, which may be a result of redistribution of these cell types to the tumor site (Supplementary Fig. S6A). Supplementary Fig. S6C and S6D show the gating strategy for this experiment.

Aggressively growing B16 tumors usually contain large areas of necrotic tissue (Fig. 4G). We noted a striking absence of necrosis in MLN8237 and MLN8237 and (−)-Nutlin-3–treated tumors. Even though the sizes of the MLN8237-treated tumors varied (Fig. 4B), the absence of necrosis was consistent, suggesting an active clearance mechanism beyond growth inhibition. To determine the significance of tumor-infiltrating immune cells in tumor clearance and overall drug response, we compared efficacy of MDM2 and AURKA inhibition against B16F0 melanoma tumors that were grown either in immunocompetent C57Bl6 mice or in severely immunodeficient NOD/SCID IL2 receptor gamma chain null (NSG) mice that lack T, B, and NK cells, have functionally defective macrophages, DCs and compromised cytokine signaling. Therapeutic efficacy was greatly reduced in immunocompromised mice as compared with immunocompetent animals (compare Fig. 4H and Fig. 4A). The induction of the apoptotic marker BIM_{EL} was comparable in immunocompetent and immunodeficient models (Supplementary Fig. S4C). In contrast, clearance of necrotic areas in senescent tumors treated with MLN8237 or MLN8237 and (−)-Nutlin-3 combination was abrogated in the absence of functional immune system (Fig. 4I). This suggests that immune cells recruited into the tumors in response to combined MDM2 and AURKA antagonism facilitate tumor clearance rather than direct melanoma cell killing. This conclusion is also supported by the data from the T-cell–deficient mouse model in which the response to senescence-inducing therapy with the AURKA inhibitor, as well as to combined AURKA and MDM2 antagonists treatment, was associated with accumulation of phagocytic myeloid cells, such as macrophages and DCs within the tumors (Supplementary Fig. S7).

Senescent cells attract immune cells through induction of senescence-associated secretory phenotype (SASP), characterized by increased secretion of proinflammatory cytokines and chemokines. We investigated which cytokines in particular orchestrated immune infiltration of tumors treated with MDM2 and AURKA

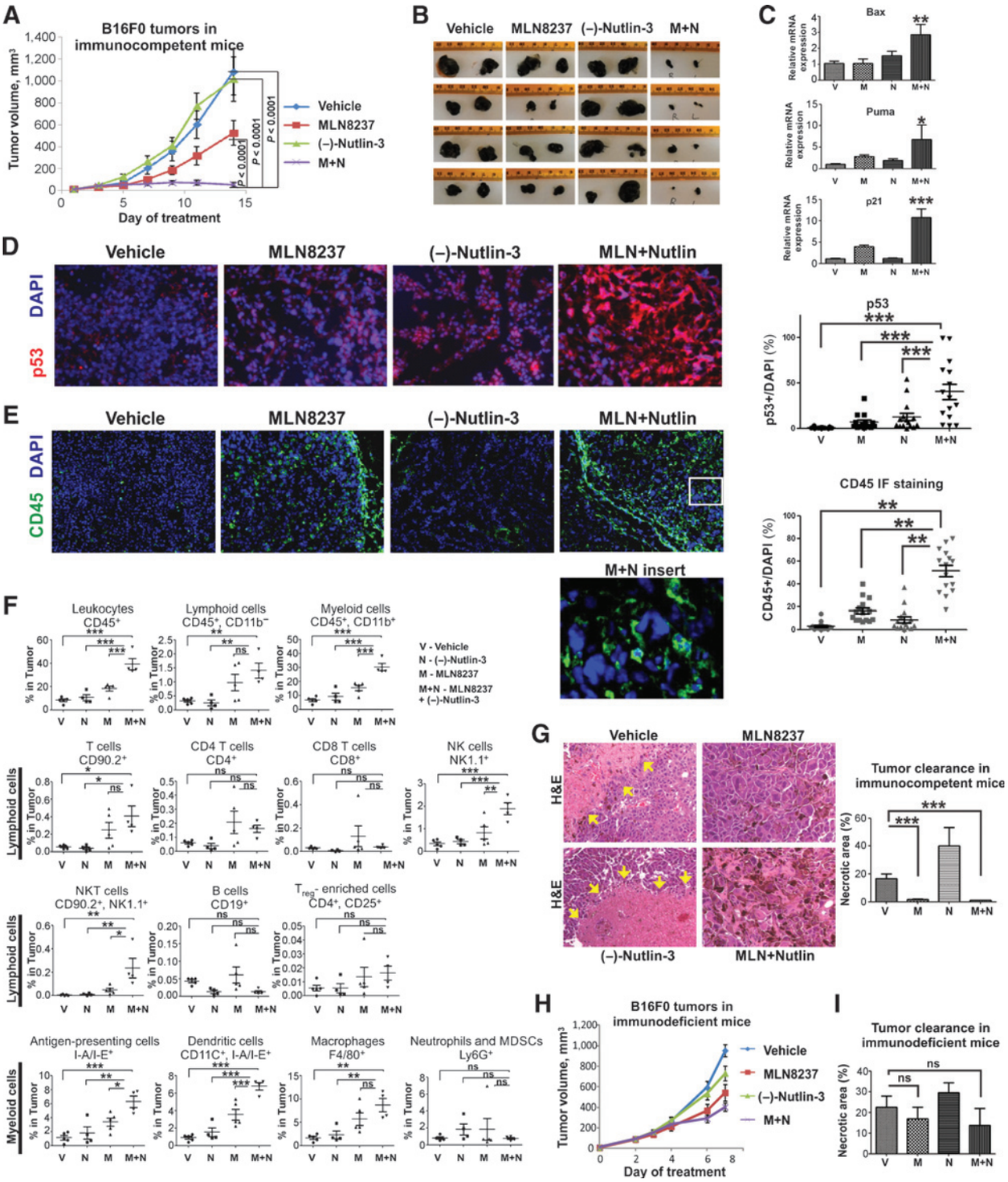

Figure 4.
Cotargeting AURKA and MDM2 promotes immune infiltration of melanoma tumors. A, growth of B16F0 tumors in C57Bl6 mice treated with (−)-Nutlin-3 (200 mg/kg), MLN8237 (30 mg/kg), combination of both, or vehicle. B, photographs of excised tumors described in A. C, real-time PCR analysis of p53 transcriptional targets p21, Bax, and Puma in tumors described in A. D, immunofluorescence staining of p53 in tumors described in A. E, immunofluorescence staining of leukocytes in tumors described in A using CD45 antibody. Quantitative analysis of staining in D and E was performed using ImageJ software; five random fields of three individual tumors were evaluated in each treatment group. F, flow cytometric analysis of indicated lymphoid and myeloid cells in tumors described in A. G, H&E staining of tumors described in A. Arrows, necrotic areas. The percentage of necrotic area in whole-tumor sections was determined by a pathologist in a blind manner (right). H, drug response in immunodeficient mice. Experiments were performed as described in A, except NSG mice were used. I, necrotic area in tumors described in H was quantified on the basis of H&E staining by pathologist in a blind manner. *, $P < 0.05$; **, $P < 0.01$; ***, $P < 0.001$; ns, not significant, $P > 0.05$.

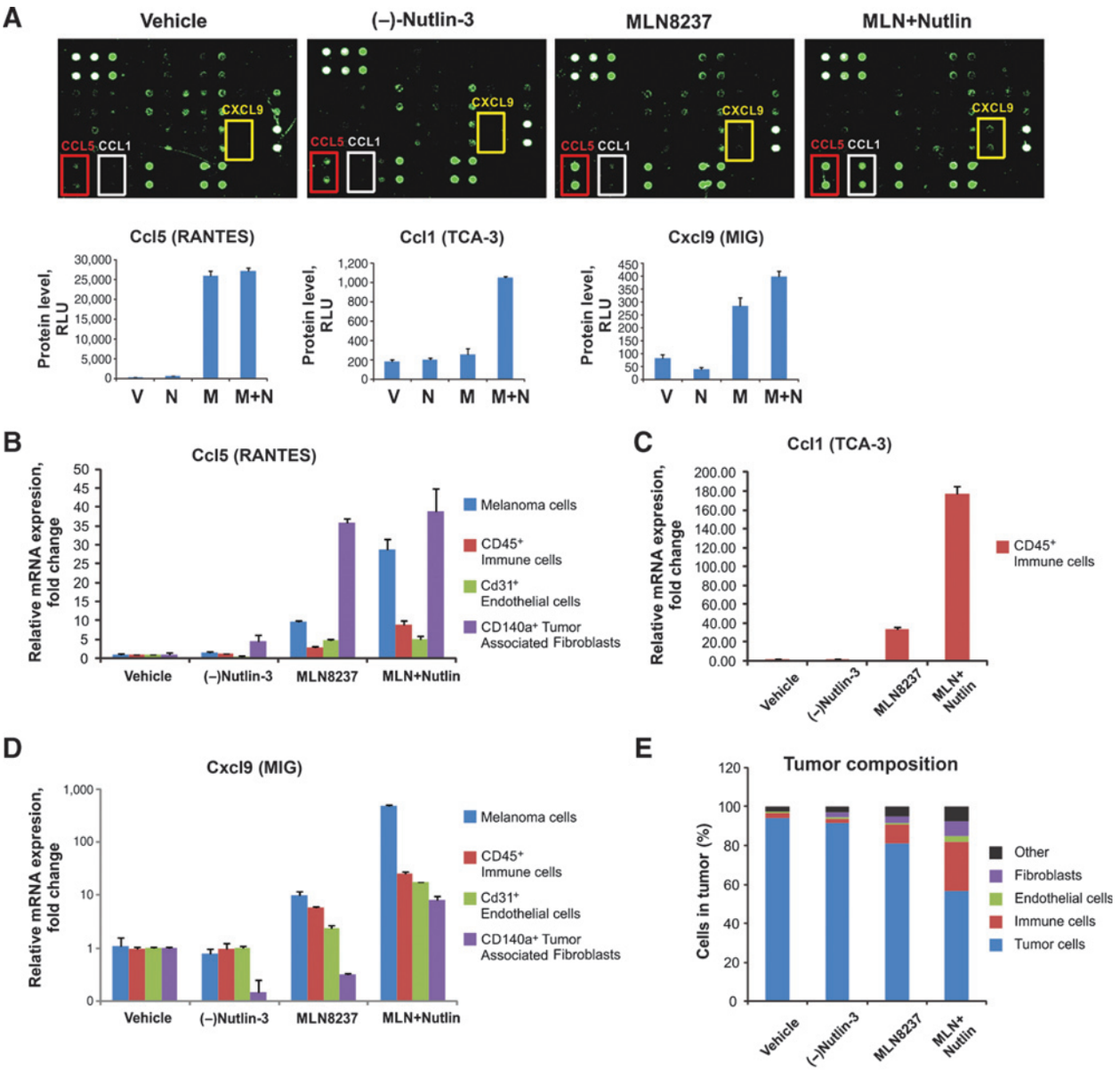

Figure 5.
MDM2 and AURKA antagonism promotes tumor immune infiltration. A, cytokine levels in tumor lysates from B16F0 tumor-bearing immunocompetent mice were detected using cytokine array (Ray Bio). Cytokines differentially expressed between the treatment groups are indicated. Bottom, quantification of the results using the manufacturer's software. B–D, levels of Ccl5, Ccl1, and Cxcl9 in different cell types within the B16F0 tumors were analyzed using qRT-PCR. Cells were collected by FACS. E, percentages of the indicated cell types in B16F0 tumors as determined by FACS analysis.

inhibitors. A prominent increase of the Ccl5 chemokine was detected in response to AURKA inhibitor treatment as well as an induction of Ccl1 and Cxcl9 in tumors treated with AURKA and MDM2 antagonists combined (Fig. 5A). Ccl5 attracts monocytes, macrophages, dendritic, and NK cells; Ccl1 recruits monocytes, dendritic, and T cells; and Cxcl9 targets T and NK cells (41). These functional characteristics are consistent with the profiles of tumor-infiltrating leukocytes in MLN8237 and (−)-Nutlin-3–treated cells (Fig. 4F).

To investigate what cell types within the tumor microenvironment (TME) were producing these chemokines, we FACS sorted immune cells, endothelial cells, fibroblasts, and melanoma cells in the tumor based on the surface markers CD45, CD31, CD140a, and analyzed their expression of Ccl1, Ccl5, and Cxcl9. Ccl5 levels were increased in both melanoma cells and fibroblasts upon MLN8237 or MLN8237 and (−)-Nutlin-3 treatments (Fig. 5B). However, because fibroblasts represented a relatively minor cell population within the TME, melanoma cells were the main source of Ccl5 in the tumor (Fig. 5E). Similarly, melanoma cells were the source of Cxcl9 upon AURKA and MDM2 cotargeting, whereas the tumor-infiltrating immune cells produced Ccl1 (Fig. 5C and D).

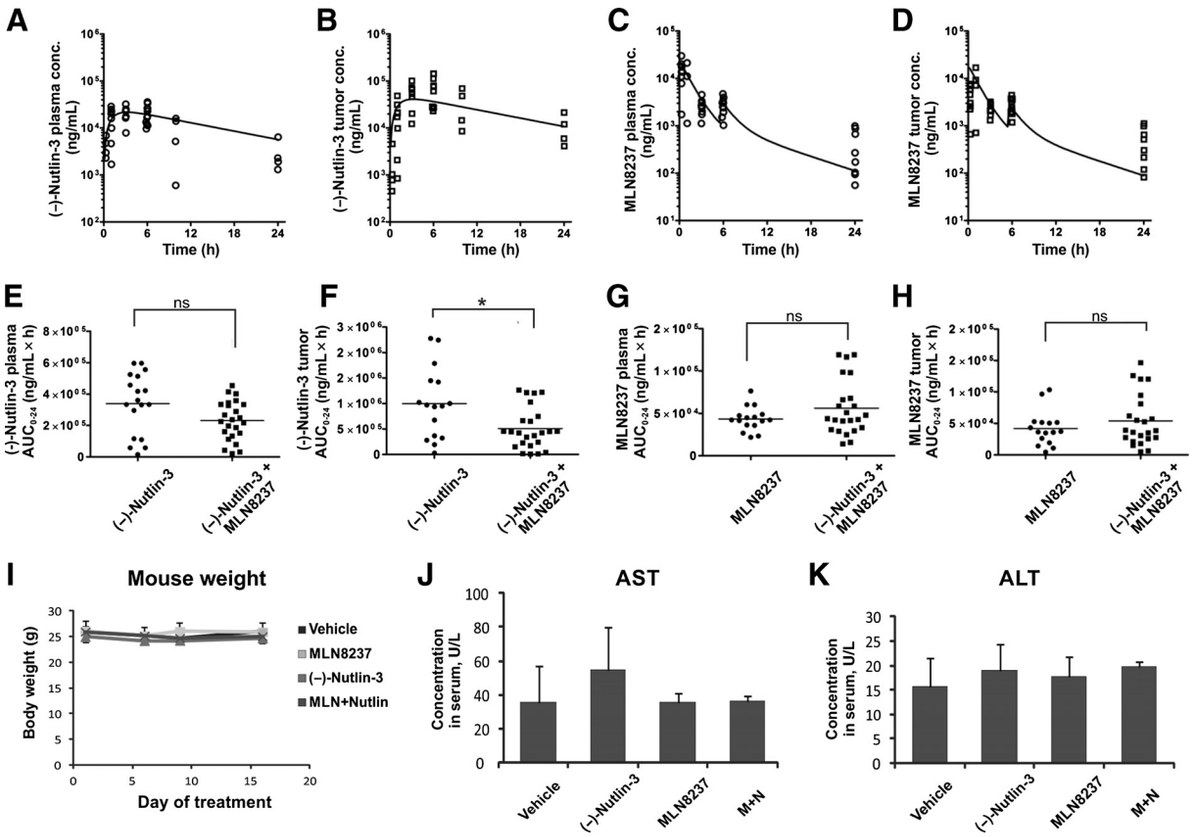

Figure 6.
(−)-Nutlin-3 and MLN8237 pharmacokinetics and safety. A–D, population model predicted (−) and observed (o) plasma and tumor concentrations of (−)-Nutlin-3 (A and B, respectively) and MLN8237 (C and D, respectively). Median (−)-Nutlin-3 and MLN8237 plasma and tumor exposure after indicated treatments. Single-agent and combination treatment groups were compared using the Mann–Whitney test (E–H). *, $P < 0.05$; ns, not significant, $P > 0.05$. Body weight and serum levels of liver toxicity markers AST and ALT in tumor-free C57Bl6 mice that received daily treatments with (−)-Nutlin-3 (200 mg/kg), MLN8237 (30 mg/kg), combination of both, or vehicle control (I–K).

(−)-Nutlin-3 and MLN8237 drug combination exhibits good bioavailability and low toxicity.

For pharmacokinetics analysis, matched plasma and tumor tissue samples from 56 B16F0 melanoma-bearing C57Bl6 mice treated with MLN8237 (30 mg/kg) and/or (−)-Nutlin-3 (200 mg/kg) were evaluated and modeled together using a population pharmacokinetic approach (Supplementary Table S1). The population model-predicted plasma and tissue concentration–time plots for (−)-Nutlin-3 (Fig. 6A and 6B) and MLN8237 (Fig. 6C and 6D) indicate adequate model fitting of the observed data. The hybrid physiologically based pharmacokinetic models for (−)-Nutlin-3 and MLN8237 are shown in Supplementary Fig. S5.

The median (−)-Nutlin-3 $AUC_{0-24\ h}$ estimate was 292.7 μg/mL × h for plasma and 455.6 μg/mL × h for tumor tissue. The overall median (range) MLN8237 area under the concentration–time curve from time 0 to 24 hours ($AUC_{0-24\ h}$) estimate was 42.7 μg/mL × h (14.0–119) for plasma and 37.4 μg/g × h (4.59–147) for tumor tissue. The median (−)-Nutlin-3 plasma $AUC_{0-24\ h}$ decreased 34% ($P = 0.0519$) in mice that received (−)-Nutlin-3 and MLN8237 compared with the (−)-Nutlin-3 single-agent arm (Fig. 6E). Likewise, Fig. 6F shows 55% reduction in the median (−)-Nutlin-3 tissue $AUC_{0-24\ h}$ ($P < 0.05$) for mice receiving concomitant MLN8237. The plasma and tumor exposure were similar comparing mice that received MLN8237 alone or combined with (−)-Nutlin-3 (Fig. 6G and 6H). These results suggest a potential interaction between (−)-Nutlin-3 and MLN8237 that reduces (−)-Nutlin-3 tumor tissue exposure. The clinical relevance of this interaction remains to be determined and further studies will be required to optimize the dosing and scheduling of these drugs as they are integrated into clinical practice. Nevertheless, the efficacy studies demonstrate excellent antitumor effect of combined (−)-Nutlin-3 and MLN8237 treatment despite the slight short-term reduction in tumor tissue levels of (−)-Nutlin-3 when combined with MLN8237.

To assess safety/potential toxicity of this drug combination, we monitored weight of laboratory animals receiving the therapy and analyzed the levels of liver toxicity markers ALT and AST in serum of treated mice. No significant weight loss or signs of liver toxicity were detected (Fig. 6 I–K).

Combined MDM2 and AURKA antagonism blocks growth of patient-derived tumors with $BRAF^{WT}$ and $BRAF^{V600E}$

To evaluate anti-melanoma activity of MDM2 and AURKA targeting in clinically relevant setting, 5 patient melanoma tumors were transplanted into nude mice creating a PDX model. Multiple studies demonstrated that PDX tumors retain the histology, gene

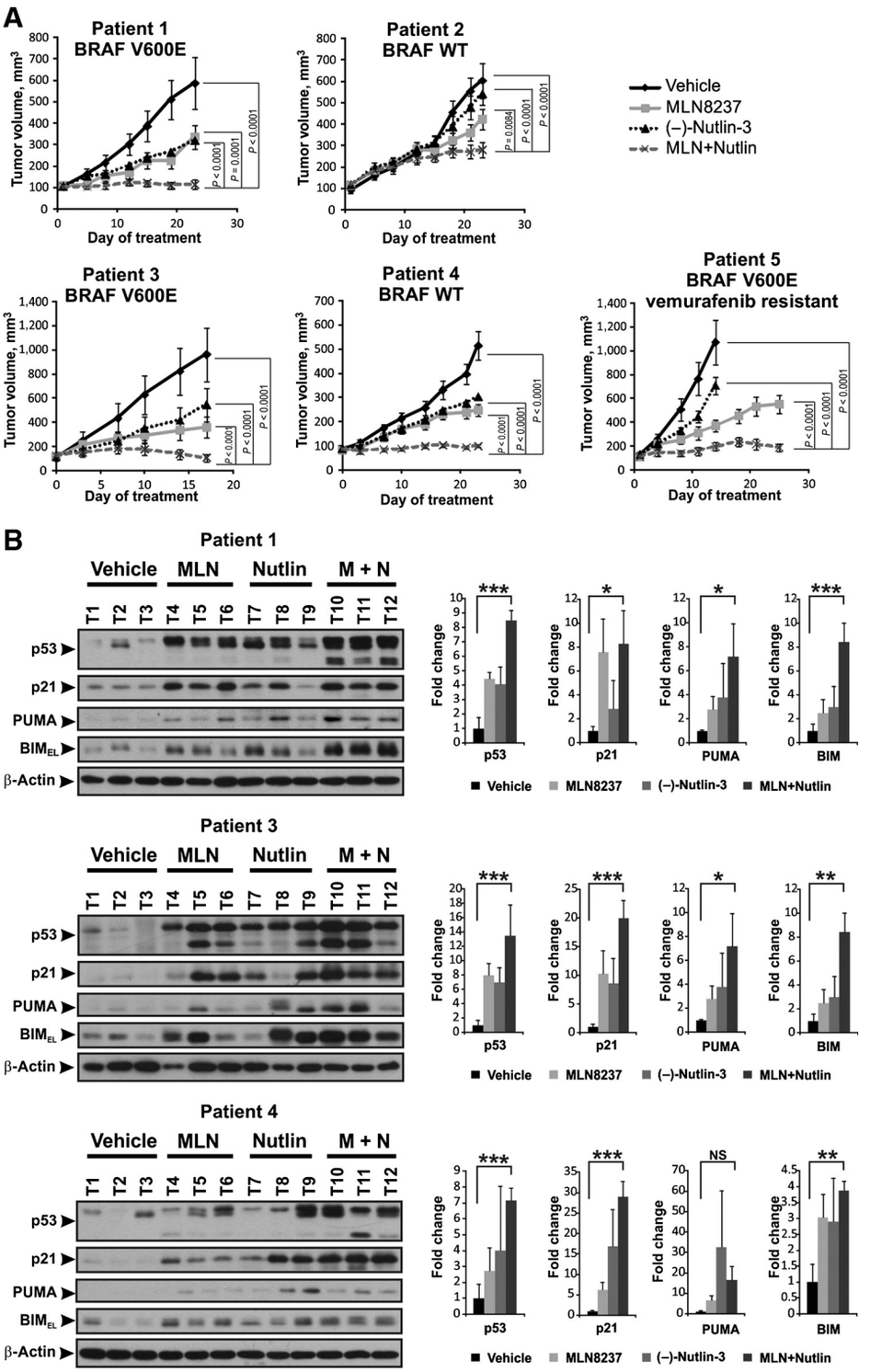

Figure 7.
Cotargeting AURKA and MDM2 blocks growth of PDX. A, mice bearing human melanoma implants (patients 1–5) received daily treatments with (−)-Nutlin-3 (200 mg/kg), MLN8237 (30 mg/kg), combination of both, or vehicle control. B, Western blot analysis of the indicated tumors shown in A. The average protein expression ± SD in each treatment group (right panels) was calculated based on the densitometry analysis. *, $P < 0.05$; **, $P < 0.01$; ***, $P < 0.001$; and ns, not significant, $P > 0.05$.

alteration, and expression profiles as well as drug response rates of their source tumors (reviewed in ref. 42), which makes them an excellent model for preclinical evaluation of new therapeutics. Our PDX set included tumors with unknown driver mutations (*BRAF*^{WT}, *c-Kit*^{WT}, and *NRAS*^{WT}; patients 2 and 4) and tumors with mutation in *BRAF* (BRAF^{V600E} patients 1, 3, and 5). Patient 5 received treatment with BRAF inhibitor vemurafenib and progressed after an initial response. All tumors were p53^{WT} based on direct sequencing of all *TP53* coding exons. Combined (−)-Nutlin-3 and MLN8237 treatment was significantly more

effective than vehicle or single-agent treatment in all experiments and fully blocked the growth of 4 of 5 tested patient tumors (Fig. 7A). Strong induction of p53, its targets p21, PUMA, and the mitochondrial apoptosis effector BIM_{EL} was observed in tumor lysates of (−)-Nutlin-3 and MLN8237-treated mice (Fig. 7B). These data suggest that combined MDM2- and AURKA-targeted therapy may benefit patients with $BRAF^{WT}$, as well as with BRAF inhibitor–resistant tumors.

Collectively, our results demonstrate that combined MDM2 and AURKA antagonism halts melanoma growth by inducing growth arrest and senescence, limiting lifespan of senescent cells, and enhancing tumor immune infiltration and clearance.

Discussion

We hypothesized that p53-restorative therapy can synergize with concurrent senescence-promoting therapy. Tumor senescence and immune-mediated tumor clearance has been linked with response to genetic p53 restoration (21, 43). However, we found that pharmacologic p53 inducer (−)-Nutlin-3 elicited cytotoxic rather than senescence response in melanoma tumors. Therefore, we combined (−)-Nutlin-3 with the AURKA antagonist MLN8237, which is capable of triggering melanoma cell senescence *in vivo* (7). Although senescence induction was found to be critical for the therapeutic efficacy of this drug, we cannot fully exclude the possibility that antimelanoma effect of AURKA inhibition extends beyond senescence. A daily oral regimen with the combination of MDM2 and AURKA inhibitors blocked the growth of patient-derived $p53^{WT}$ melanoma tumors independent of BRAF mutational status or resistance to BRAF inhibitor. These data suggest that p53-restoring mitotic kinase–targeted therapy could benefit patients with melanoma who are not eligible for BRAF and MEK inhibitors. Because both p53-activating drugs and mitotic kinase inhibitors have already been tried on human subjects, prompt translation of combination therapy to the clinic is highly feasible.

Although (−)-Nutlin-3 alone was a modest inducer of p53 *in vivo*, addition of AURKA inhibitor promoted p53 activation in tumors. This is in agreement with studies showing that AURKA phosphorylates p53 on serine 315 and 215, which leads to MDM2-dependent p53 ubiquitination and degradation with inhibition of p53 transcriptional activity (44, 45). Consistent with previous findings in hepatocellular carcinoma and sarcoma (21, 43), p53 activation failed to initiate classical caspase-driven apoptosis in melanoma. Nevertheless, we noted a delayed caspase-independent cytotoxic response that may have been previously overlooked. Prolonged p53 activation in melanoma cells resulted in mitochondrial dysfunction and mitochondrial-nuclear translocation of AIF, a known mediator of caspase-independent cell death (35).

Accumulating evidence suggests that the TME can be an important positive or negative determinant of tumor response to therapy. For example, stromal cells have been implicated in the protection of tumor cells from MEK and BRAF inhibitor–induced toxicity in melanoma (46). Other studies showed that treatment with BRAF and MEK inhibitors restores function to compromised DC and T cells, thus establishing a tumor-suppressing TME (47, 48). We found that nonmalignant cells in the TME can modulate the efficacy of p53-restorative therapy. Senescence induced by AURKA inhibition promoted accumulation of immune cells in melanoma tumors. These findings are in agreement with the critical role of immune cells in targeted elimination of senescent premalignant cells, as well as clearance of senescent tumor cells (49). As we reported previously, AURKA inhibition in melanoma cells initiates SASP driven in part by NF-κB activity (7). Interestingly, activation of p53 in senescent AURKA-deficient tumors further promoted recruitment of macrophages, DCs, and NK cells by costimulating the expression of Ccl5, Ccl1, and Cxcl9 chemokines in malignant and nonmalignant cells of TME. These results are in concert with a recent finding that p53 can cooperate with NF-κB in SASP induction (50). Compromised antitumor activity of AURKA and MDM2 antagonism in severely immunodeficient animals indicates that immune-mediated tumor clearance plays a critical role in response to this therapy.

Our study demonstrates that the potent therapeutic benefit of MDM2 and AURKA cotargeting is derived from a direct effect on melanoma cells combined with stimulation of host's antitumor defenses. Activation of p53 synergized with AURKA antagonism to inhibit growth and survival of melanoma cells and promote immune-mediated tumor clearance. These findings provide a strong rationale to further develop p53-reactivating therapies in combination with senescence-inducing drugs, for instance, mitotic kinase inhibitors, for treatment of $p53^{WT}$ metastatic melanoma.

Disclosure of Potential Conflicts of Interest

M.C. Kelley reports receiving a commercial research grant from GSK/NCCN, is a consultant/advisory board member for Amgen and has provided expert testimony for multiple clinical professional liability cases—expert witness. No potential conflicts of interest were disclosed by the other authors.

Authors' Contributions

Conception and design: A.E. Vilgelm, G.D. Ayers, J.A. Sosman, M.C. Kelley, A. Richmond

Development of methodology: A.E. Vilgelm, O.E. Hawkins, K.P. Weller, D.C. Turner, J.A. Ecsedy, A. Richmond

Acquisition of data (provided animals, acquired and managed patients, provided facilities, etc.): A.E. Vilgelm, J.S. Pawlikowski, Y. Liu, O.E. Hawkins, J. Smith, K.P. Weller, L.W. Horton, D.C. Turner, D.C. Essaka

Analysis and interpretation of data (e.g., statistical analysis, biostatistics, computational analysis): A.E. Vilgelm, G.D. Ayers, D.C. Turner, C.F. Stewart, J.A. Ecsedy, A. Richmond

Writing, review, and/or revision of the manuscript: A.E. Vilgelm, Y. Liu, D.C. Turner, C.F. Stewart, J.A. Sosman, M.C. Kelley, J.A. Ecsedy, J.N. Johnston, A. Richmond

Administrative, technical, or material support (i.e., reporting or organizing data, constructing databases): T.A. Davis, L.W. Horton, C.M. McClain, J.N. Johnston, A. Richmond

Study supervision: A. Richmond

Other (tissue acquisition for human tumor xenografts, clinical information regarding molecular phenotype, disease course, and response to therapy): M.C. Kelley

Other (chemical synthesis, supervision of chemistry-related aspects of the study): J.N. Johnston

Grant Support

This work was supported by grants from the Department of Veterans Affairs (5101BX000196-04), NIH (CA116021, CA116021-S1, CA90625, 5T32CA119925-03, 1F32CA171895-01, GM084333, and CA68485), and a senior research career scientist award to A. Richmond.

The costs of publication of this article were defrayed in part by the payment of page charges. This article must therefore be hereby marked *advertisement* in accordance with 18 U.S.C. Section 1734 solely to indicate this fact.

Received August 19, 2014; revised October 24, 2014; accepted October 29, 2014; published OnlineFirst November 14, 2014.

References

1. Chapman PB, Hauschild A, Robert C, Haanen JB, Ascierto P, Larkin J, et al. Improved survival with vemurafenib in melanoma with BRAF V600E mutation. N Engl J Med 2011;364:2507–16.
2. Sosman JA, Kim KB, Schuchter L, Gonzalez R, Pavlick AC, Weber JS, et al. Survival in BRAF V600-mutant advanced melanoma treated with vemurafenib. N Engl J Med 2012;366:707–14.
3. Hauschild A, Grob JJ, Demidov LV, Jouary T, Gutzmer R, Millward M, et al. Dabrafenib in BRAF-mutated metastatic melanoma: a multicentre, open-label, phase 3 randomised controlled trial. Lancet 2012;380: 358–65.
4. Flaherty KT, Infante JR, Daud A, Gonzalez R, Kefford RF, Sosman J, et al. Combined BRAF and MEK inhibition in melanoma with BRAF V600 mutations. N Engl J Med 2012;367:1694–703.
5. Menzies AM, Long GV. Dabrafenib and trametinib, alone and in combination for BRAF-mutant metastatic melanoma. Clin Cancer Res 2014; 20:2035–43.
6. Matulonis UA, Sharma S, Ghamande S, Gordon MS, Del Prete SA, Ray-Coquard I, et al. Phase II study of MLN8237 (alisertib), an investigational Aurora A kinase inhibitor, in patients with platinum-resistant or -refractory epithelial ovarian, fallopian tube, or primary peritoneal carcinoma. Gynecol Oncol 2012;127:63–9.
7. Liu Y, Hawkins OE, Su Y, Vilgelm AE, Sobolik T, Thu YM, et al. Targeting aurora kinases limits tumour growth through DNA damage-mediated senescence and blockade of NF-kappaB impairs this drug-induced senescence. EMBO Mol Med 2013;5:149–66.
8. Junttila MR, Evan GI. p53–a Jack of all trades but master of none. Nat Rev Cancer 2009;9:821–9.
9. Goel VK, Ibrahim N, Jiang G, Singhal M, Fee S, Flotte T, et al. Melanocytic nevus-like hyperplasia and melanoma in transgenic BRAFV600E mice. Oncogene 2009;28:2289–98.
10. Bardeesy N, Bastian BC, Hezel A, Pinkel D, DePinho RA, Chin L. Dual inactivation of RB and p53 pathways in RAS-induced melanomas. Mol Cell Biol 2001;21:2144–53.
11. Gembarska A, Luciani F, Fedele C, Russell EA, Dewaele M, Villar S, et al. MDM4 is a key therapeutic target in cutaneous melanoma. Nat Med 2012;18:1239–47.
12. Terzian T, Torchia EC, Dai D, Robinson SE, Murao K, Stiegmann RA, et al. p53 prevents progression of nevi to melanoma predominantly through cell cycle regulation. Pigment Cell Melanoma Res 2010;23:781–94.
13. Hodis E, Watson IR, Kryukov GV, Arold ST, Imielinski M, Theurillat JP, et al. A landscape of driver mutations in melanoma. Cell 2012;150:251–63.
14. Cerami E, Gao J, Dogrusoz U, Gross BE, Sumer SO, Aksoy BA, et al. The cBio cancer genomics portal: an open platform for exploring multidimensional cancer genomics data. Cancer Discov 2012;2:401–4.
15. Goldstein AM, Chan M, Harland M, Hayward NK, Demenais F, Bishop DT, et al. Features associated with germline CDKN2A mutations: a GenoMEL study of melanoma-prone families from three continents. J Med Genet 2007;44:99–106.
16. Freedberg DE, Rigas SH, Russak J, Gai W, Kaplow M, Osman I, et al. Frequent p16-independent inactivation of p14ARF in human melanoma. J Natl Cancer Inst 2008;100:784–95.
17. Kubbutat MH, Ludwig RL, Ashcroft M, Vousden KH. Regulation of Mdm2-directed degradation by the C terminus of p53. Mol Cell Biol 1998;18: 5690–8.
18. Gray-Schopfer V, Wellbrock C, Marais R. Melanoma biology and new targeted therapy. Nature 2007;445:851–7.
19. Carry JC, Garcia-Echeverria C. Inhibitors of the p53/hdm2 protein–protein interaction-path to the clinic. Bioorg Med Chem Lett 2013;23:2480–5.
20. Lu M, Breyssens H, Salter V, Zhong S, Hu Y, Baer C, et al. Restoring p53 function in human melanoma cells by inhibiting MDM2 and cyclin B1/CDK1-phosphorylated nuclear iASPP. Cancer Cell 2013;23:618–33.
21. Xue W, Zender L, Miething C, Dickins RA, Hernando E, Krizhanovsky V, et al. Senescence and tumour clearance is triggered by p53 restoration in murine liver carcinomas. Nature 2007;445:656–60.
22. Su Y, Vilgelm AE, Kelley MC, Hawkins OE, Liu Y, Boyd KL, et al. RAF265 inhibits the growth of advanced human melanoma tumors. Clin Cancer Res 2012;18:2184–98.
23. Davis TA, Vilgelm AE, Richmond A, Johnston JN. Preparation of (-)-nutlin-3 using enantioselective organocatalysis at decagram scale. J Org Chem 2013;78:10605–16.
24. Bai F, Zhu F, Tagen M, Miller L, Owens TS, Mallari J, et al. Determination of nutlin-3a in murine plasma by liquid chromatography electrospray ionization tandem mass spectrometry (LC-ESI-MS/MS). J Pharm Biomed Anal 2010;51:915–20.
25. Bauer RJ, Guzy S, Ng C. A survey of population analysis methods and software for complex pharmacokinetic and pharmacodynamic models with examples. AAPS J 2007;9:E60–83.
26. Brown RP, Delp MD, Lindstedt SL, Rhomberg LR, Beliles RP. Physiological parameter values for physiologically based pharmacokinetic models. Toxicol Ind Health 1997;13:407–84.
27. Wang E. Senescent human fibroblasts resist programmed cell death, and failure to suppress bcl2 is involved. Cancer Res 1995;55:2284–92.
28. Yeo EJ, Hwang YC, Kang CM, Choy HE, Park SC. Reduction of UV-induced cell death in the human senescent fibroblasts. Mol Cells 2000;10:415–22.
29. Seluanov A, Gorbunova V, Falcovitz A, Sigal A, Milyavsky M, Zurer I, et al. Change of the death pathway in senescent human fibroblasts in response to DNA damage is caused by an inability to stabilize p53. Mol Cell Biol 2001;21:1552–64.
30. Sanders YY, Liu H, Zhang X, Hecker L, Bernard K, Desai L, et al. Histone modifications in senescence-associated resistance to apoptosis by oxidative stress. Redox Biol 2013;1:8–16.
31. Uberti D, Carsana T, Bernardi E, Rodella L, Grigolato P, Lanni C, et al. Selective impairment of p53-mediated cell death in fibroblasts from sporadic Alzheimer's disease patients. J Cell Sci 2002;115:3131–8.
32. Gorgun G, Calabrese E, Hideshima T, Ecsedy J, Perrone G, Mani M, et al. A novel Aurora-A kinase inhibitor MLN8237 induces cytotoxicity and cell-cycle arrest in multiple myeloma. Blood 2010;115:5202–13.
33. Vassilev LT, Vu BT, Graves B, Carvajal D, Podlaski F, Filipovic Z, et al. *In vivo* activation of the p53 pathway by small-molecule antagonists of MDM2. Science 2004;303:844–8.
34. Vousden KH, Lu X. Live or let die: the cell's response to p53. Nat Rev Cancer 2002;2:594–604.
35. Cande C, Vahsen N, Garrido C, Kroemer G. Apoptosis-inducing factor (AIF): caspase-independent after all. Cell Death Differ 2004;11:591–5.
36. Bourdon JC, Fernandes K, Murray-Zmijewski F, Liu G, Diot A, Xirodimas DP, et al. p53 isoforms can regulate p53 transcriptional activity. Genes Dev 2005;19:2122–37.
37. Secchiero P, Corallini F, Gonelli A, Dell'Eva R, Vitale M, Capitani S, et al. Antiangiogenic activity of the MDM2 antagonist nutlin-3. Circ Res 2007;100:61–9.
38. Bhattacharya A, Toth K, Mazurchuk R, Spernyak JA, Slocum HK, Pendyala L, et al. Lack of microvessels in well-differentiated regions of human head and neck squamous cell carcinoma A253 associated with functional magnetic resonance imaging detectable hypoxia, limited drug delivery, and resistance to irinotecan therapy. Clin Cancer Res 2004;10:8005–17.
39. Primeau AJ, Rendon A, Hedley D, Lilge L, Tannock IF. The distribution of the anticancer drug Doxorubicin in relation to blood vessels in solid tumors. Clin Cancer Res 2005;11:8782–8.
40. Minchinton AI, Tannock IF. Drug penetration in solid tumours. Nat Rev Cancer 2006;6:583–92.
41. Bonecchi R, Galliera E, Borroni EM, Corsi MM, Locati M, Mantovani A. Chemokines and chemokine receptors: an overview. Circ Res 2009;14: 540–51.
42. Tentler JJ, Tan AC, Weekes CD, Jimeno A, Leong S, Pitts TM, et al. Patient-derived tumour xenografts as models for oncology drug development. Nat Rev Clin Oncol 2012;9:338–50.
43. Ventura A, Kirsch DG, McLaughlin ME, Tuveson DA, Grimm J, Lintault L, et al. Restoration of p53 function leads to tumour regression *in vivo*. Nature 2007;445:661–5.
44. Katayama H, Sasai K, Kawai H, Yuan ZM, Bondaruk J, Suzuki F, et al. Phosphorylation by aurora kinase A induces Mdm2-mediated destabilization and inhibition of p53. Nat Genet 2004;36:55–62.
45. Liu Q, Kaneko S, Yang L, Feldman RI, Nicosia SV, Chen J, et al. Aurora-A abrogation of p53 DNA binding and transactivation activity by phosphorylation of serine 215. J Biol Chem 2004;279:52175–82.
46. Straussman R, Morikawa T, Shee K, Barzily-Rokni M, Qian ZR, Du J, et al. Tumour micro-environment elicits innate resistance to RAF inhibitors through HGF secretion. Nature 2012;487:500–4.
47. Ott PA, Henry T, Baranda SJ, Frleta D, Manches O, Bogunovic D, et al. Inhibition of both BRAF and MEK in BRAF(V600E) mutant melanoma

restores compromised dendritic cell (DC) function while having differential direct effects on DC properties. Cancer Immunol Immunother 2013;62:811–22.
48. Frederick DT, Piris A, Cogdill AP, Cooper ZA, Lezcano C, Ferrone CR, et al. BRAF inhibition is associated with enhanced melanoma antigen expression and a more favorable tumor microenvironment in patients with metastatic melanoma. Clin Cancer Res 2013;19:1225–31.
49. Serrano M. Cancer: final act of senescence. Nature 2011;479:481–2.
50. Lujambio A, Akkari L, Simon J, Grace D, Tschaharganeh DF, Bolden JE, et al. Non-cell-autonomous tumor suppression by p53. Cell 2013;153:449–60.